Monitoring Spatiotemporal Expansion Dynamics of Short-Rotation Eucalyptus Plantations Over Large Scales Using Landsat Time-Series Data

Yuanzheng Yang, Wen H. Cai, Qiuxia Huang, Le Yu, Jiaxing Zu, Jiali Wang, and Jian Yang

***Abstract*—Eucalyptus, valued for its rapid growth and economic potential, has been widely introduced in China to address timber demands while conserving natural forests. Precisely estimating the spatiotemporal expansion of short-rotation eucalyptus plantations is crucial for evaluating their ecological and social value and formulating effective sustainable forestry policies. Medium-resolution satellite images, such as Landsat data, offer a cost-effective tool for large-scale forest mapping compared with the traditional forest inventories. This study used pixel-level time-series analysis to identify annual eucalyptus plantation distributions across Guangxi, China, from 2004 to 2019, based on the standard temporal vegetation index curves derived from the characteristics of short-rotation and fast-growing eucalyptus. Furthermore, an image segmentation method, coupled with an empirical relationship linking patch-level landscape indices to optimal thresholds, was employed to eliminate isolated pixels and reduce omission errors arising from the above time-series analysis. The established thresholds increased the accurate identification of eucalyptus patches within segments. Our proposed eucalyptus detection algorithm achieved an overall accuracy exceeding 80%, demonstrating its effectiveness. The analysis revealed eucalyptus plantations increased from 0.42×10^6 ha in 2004 to 2.47×10^6 ha in 2019, exhibiting a pronounced northward expansion. Initially concentrated in upland areas, plantations subsequently expanded into flatter terrains, raising concerns about potential agricultural conflicts. Annual eucalyptus plantation maps offer critical information for sustainable forest management and policymaking. This study highlights the potential of medium-resolution satellite data and time-series analysis for robust and cost-effective monitoring of annual short-rotation timber forest expansion dynamics over large scales.**

***Index Terms*—Eucalyptus, forest monitoring, Google Earth engine (GEE), short-rotation plantations, time-series analysis.**

I. Introduction

In RECENT decades, short-rotation eucalyptus plantations have experienced rapid expansion to meet the growing demand for wood resources [1], [2]. While this expansion offers significant economic benefits [3], [4], its potential allelopathic effects and intensive cultivation practices, such as short rotations and clearcut logging, also raise concerns about ecological impacts [5], [6], [7]. The accurate and up-to-date monitoring of eucalyptus plantation distribution is crucial for assessing their environmental consequences [8]. Previous studies have reported statistical data about eucalyptus plantation area in specific years or at local scales [9], [10], [11]. However, comprehensive information regarding the magnitude, spatial distribution, and temporal trends of eucalyptus plantation expansion in China remains poorly documented. This lack of information hinders our ability to predict future expansion trajectory and develop sustainable forest management practices.

Remote sensing offers an effective and economical way to document annual plantation expansion dynamics across large scales [13], [14]. Several approaches have been explored to recognize tree species using the spectrum information acquired from high spatial resolution images, which could delineate the distinctive canopy structure [15], [16], [17], while others explored the biochemical properties and/or leaf morphology variation of different tree species in spectrum using hyperspectral data [18], [19], [20]. Single or combined high-resolution images and hyperspectral data can provide comprehensive information on feature texture and spectral properties, exhibiting a solid performance in plantation classification [10], [15], [21], [22]. However, high spatial resolution images and hyperspectral data are associated with significant costs and are typically constrained by limited temporal coverage because such satellite systems are deployed only recently, which limits their application in large-scale, long-term forest monitoring [23], [24], [25]. Coarse-resolution time-series satellite data have been a common alternative for forest disturbance detection and classification due to their accessibility and extensive temporal coverage [13], [26].

Received 14 April 2024; revised 11 August 2024 and 18 September 2024; accepted 23 September 2024. Date of publication 1 October 2024; date of current version 23 October 2024. This work was supported in part by the National Natural Science Foundation of China under Grant 32460289, Grant 41961037, and Grant 42001216, in part by the Special Research Project of Guangxi for Research Bases and Talents under Grant AD19110143, Grant AD20297066, and Grant AD21220088, and in part by the BaGui Scholars Program of Guangxi Zhuang Autonomous Region. *(Corresponding author: Jian Yang.)*

Yuanzheng Yang, Wen H. Cai, Jiaxing Zu, and Jiali Wang are with the Key Laboratory of Environment Change and Resources Use in Beibu Gulf, Nanning Normal University, Nanning 530001, China (e-mail: yangyz@nnnu.edu.cn; caiwh@nnnu.edu.cn; zujiaxing@nnnu.edu.cn; wangjiali@nnnu.edu.cn).

Qiuxia Huang is with the College of History Culture and Tourism, Guangxi Minzu Normal University, Chongzuo 532200, China (e-mail: huangqiuxia@gxnun.edu.cn).

Le Yu is with the Department of Earth System Science, Tsinghua University, Beijing 100084, China, also with the Ministry of Education Key Laboratory for Earth System Modeling, Tsinghua University, Beijing 100084, China, also with the Institute for Global Change Studies, Tsinghua University, Beijing 100084, China, also with the Ministry of Education Ecological Field Station for East Asian Migratory Birds, Beijing 100084, China, and also with the Xi'an Institute of Surveying and Mapping Joint Research Center for Next-Generation Smart Mapping, Beijing 100084, China (e-mail: leyu@tsinghua.edu.cn).

Jian Yang is with the Department of Forestry and Natural Resources, University of Kentucky, Lexington, KY 40546 USA (e-mail: jian.yang@uky.edu).

Digital Object Identifier 10.1109/JSTARS.2024.3472008

However, its effectiveness may be inadequate in heterogeneous landscapes with fragmented patches managed by plenteous local farmers. Therefore, investigating the effectiveness of freely available satellite data with medium resolution (e.g., Landsat series data) for annual eucalyptus plantation mapping at large scales remains needed. This research aims to address this gap by exploring the feasibility and accuracy of using Landsat time-series data for monitoring eucalyptus expansion dynamics in diverse landscape settings.

To effectively identify timber plantations, researchers have explored utilizing time-series analysis of satellite imagery, capitalizing on the cyclical spectral changes associated with periodic planting and logging [27], [28]. Short-rotation eucalyptus plantations, for instance, exhibit a distinct "shark-tooth" pattern in their vegetation index, plummeting after clearcut and rapidly rising after replanting or sprouting until the next clearcut cycle [9], [10]. Time-series analysis allows for the detection of these abrupt spectral shifts triggered by clearcut events [13], [29], [30], [31]. However, cloud contamination and image acquisition limitations can lead to data gaps in satellite-based vegetation indices. Furthermore, moderate resolution pixels may contain a mixture of different features or a mix of eucalyptus plantations with different stand ages due to the piecemeal clearcutting driven by ownership fragmentation, causing deviations from the ideal "shark-tooth" pattern in the time-series curve. Relying solely on this standard curve for target feature identification can lead to misestimating, mostly underestimation [9], [32].

To address the limitations posed by the pixel-level clearcutting detection, several studies have proposed incorporating superpixel (i.e., segment) classification methods as complementary to the existing time-series analysis approach for plantation forest mapping [9], [33]. Such an integrative framework can effectively overcome challenges with isolated pixels and fragmented patches by adding two refinement steps per segment. Segments with fewer than a predefined minimum threshold of contiguous plantation forest pixels are discarded to eliminate noise, preventing "salt-and-pepper" effects. Conversely, segments surpassing a predefined threshold in proportion of identified pixels are entirely classified as a plantation forest patch, ensuring the accurate detection within large clearcuts. This approach is based on the assumption that if the identified area detected by the standard time-series curve exhibits concentrated distribution, neighboring pixels with similar spectral information have a higher probability of belonging to the same class.

A major challenge lies in establishing a threshold value above, which a pixel is classified as the target feature. Previous studies have utilized field survey data to determine optimal threshold values, through balancing omission and commission errors [9], [10]. While this approach could achieve high classification accuracy, its dependence on large volumes of training samples, especially for historical years lacking high-resolution images, limits its applicability for long-term, large-scale eucalyptus detection. In mapping the spatial distribution of Chinese maize plantation across 20 years, Peng et al. [34] proposed an "area-matching" method to iteratively adjust this threshold value until the mapped plantation area matched the reported statistics computed at the province and county levels. However, this method is still infeasible for years lacking such statistics. We propose a novel approach to develop an empirical relationship between the optimal threshold and landscape metrics of the identified plantation area estimated by time-series analysis. By exploring this relationship, it is expected to fill the gap in years lacking plantation area statistics, enabling robust and long-term eucalyptus plantation identification across large scales.

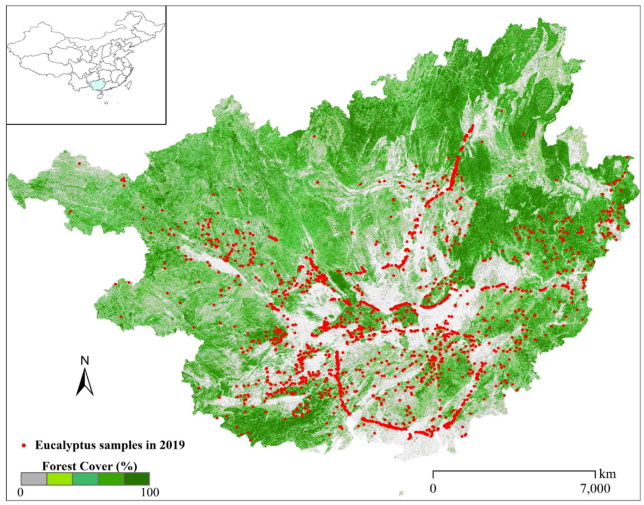

Fig. 1. Study area. Red dots indicate the eucalyptus samples collected in 2019 through field survey and visual interpretation of Google Earth imagery.

Eucalyptus plantations are extensively cultivated in China's tropical and subtropical regions, particularly in Guangxi province. However, accurately identifying these plantations on an annual basis remains a significant challenge due to the region's complex and diverse vegetation types, including exotic species with similar spectral and seasonal characteristics. Our research objectives are threefold:

1) improve a clearcut-detection-based annual eucalyptus plantation identification approach with the improved segmentation refinement method;
2) evaluate the performance of time-series analysis in identifying short-rotation eucalyptus plantations using a single data source (Landsat series datasets);
3) develop annual eucalyptus plantation distribution datasets for Guangxi, China, from 2004 to 2019.

By achieving these objectives, this study will contribute to a deeper understanding of the long-term expansion dynamics of short-rotation eucalyptus plantations in China. This knowledge and the resulting dataset can be instrumental in developing effective forest management strategies for the region.

II. Study Area

Guangxi province, located in Southwest China (20°54′N–26°24′N and 104°26′E–112°04′E), falls within the subtropical monsoon climate zone (see Fig. 1). Vegetation type in this study area is complex, including natural forests, planted forests (e.g., eucalyptus, pine, and fir), croplands (e.g., paddy fields and sugarcane fields), and orchards (e.g., citrus, lychee, and mango).

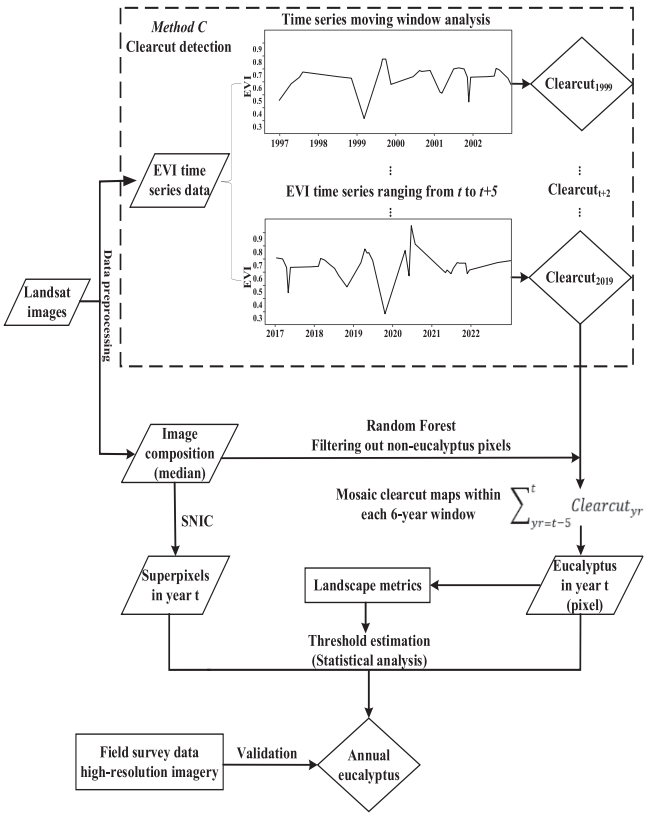

Fig. 2. Image processing and analysis flow.

The warm and humid climate provides ideal conditions for plantation growth, making Guangxi the leading timber producer in China. Eucalyptus (*Eucalyptus robusta* Smith) dominates the timber forest landscape and accounts for 2.33 million ha in 2020 [35]. Other major species of planted forests include pine (*Pinus massoniana* Lamb.) and fir (*Cunninghamia lanceolata* (Lamb.) Hook.). These plantations undergo clearcut at different intervals. Eucalyptus plantations follow a short-rotation cycle of 4–6 years, significantly shorter than fir (20–25 years) and pine (25–30 years) rotations [36], [37]. While eucalyptus plantations often display contiguous distribution and undergo successive rotations, the plantation patch size and stand age vary considerably. This can be attributed to the diverse ownership structure, with most plantations managed by individual households (local peasants) alongside state-owned forest farms. Annual eucalyptus plantation mapping provides valuable information for assessing their economic and environmental impacts, contributing to sustainable management practices in Guangxi Province.

III. Method

A. Overview

Our method is mainly derived from the study of the authors in [9] and [10] with modifications in algorithms for identifying harvesting events using the time-series analysis and choosing optimized threshold values to refine the classification after image segmentation (see Fig. 2). The overall method begins with the identification of clearcut events throughout the investigation years at the pixel level via the time-series analysis. We then utilize the harvesting rotation characteristics of eucalyptus plantation forests to determine, for each year, whether a pixel corresponds to a eucalyptus plantation based on the presence of one or two harvesting events in the preceding six years, given the 4–6 year-logging rotation of eucalyptus plantations in Guangxi province. Subsequently, we apply an image segmentation method to eliminate isolated pixels and reduce omission errors for potential eucalyptus forests that deviate from the ideal harvesting/regrowth time-series curve.

Our annual eucalyptus plantation mapping process encompasses four key steps:

1) data preparation (Landsat data assembling, preprocessing, and generating time-series vegetation index datasets);
2) clearcut detection (employing time-series analysis to identify plantation forest distribution areas);
3) eucalyptus identification (distinguishing eucalyptus plantations from other planted forest types);
4) image segmentation-based refinement for further enhancing mapping accuracy.

The validation of these eucalyptus plantation maps is described in Section III-F. We utilized Google Earth engine (GEE) as data processing platform for the entire eucalyptus plantation identification procedure, python for following data stack, and R software for statistical analysis.

B. Data Preparation

All available Landsat surface reflectance data ranging from the year 1997 to 2022 were assembled in GEE, including Landsat thematic mapper (TM), enhanced TM plus, operational land imager (OLI), and OLI-2. A total of 18 WRS path/row combinations were necessary to cover the entire Guangxi province [see Fig. 3(a)]. Preprocessing was conducted for the following classification analysis. First, the cloud and cloud shadow of each Landsat scene were removed using an automated masking algorithm. Second, an enhanced vegetation index (EVI) time series was calculated from Landsat image collection, which was used to detect clearcut disturbance (refer to Section III-C for the specific algorithm). Restricted by frequent cloud contamination in this study area [see Fig. 3(b)], the EVI time series in some pixels was discontinuous. To filter out discontinuous gaps in time series caused by cloud contamination or other noises, the EVI time series in each pixel was restructured by median value for every three-month period, resulting in four data points per year for the 1997–2022 period.

C. Clearcut Detection

Compared with commonly used vegetation indices, such as the normalized difference vegetation index, EVI exhibits greater sensitivity to foliar cover in subtropical and tropical regions, facilitating the detection of abrupt declines associated with clearcutting [38], [39]. While other vegetation indices, including the normalized burn ratio and land surface water index, have been utilized to monitor disturbances and forest recovery due to their sensitivity to topsoil exposure after disturbance [40], [41],

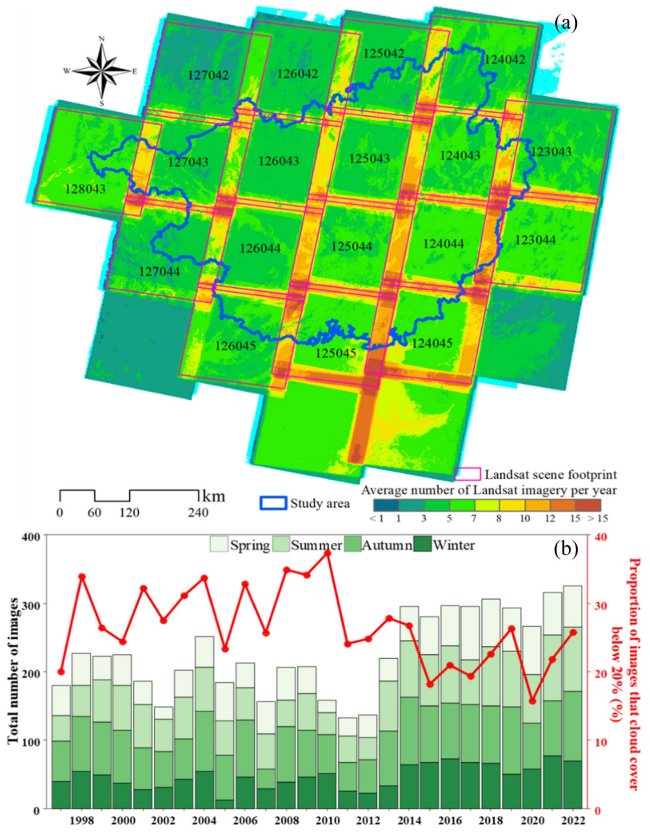

Fig. 3. Statistics of Landsat images across the study area from 1997 to 2022. (a) indicates image availability in each pixel over the past 26 years. (b) indicates the temporal and seasonal distribution during the years from 1997 to 2022, and its effective proportion (cloud cover below 30%).

[42], EVI distinguishes itself through its robustness to disturbances and its capacity to minimize the influence of atmospheric conditions and soil background on the vegetation signal [38]. The EVI is calculated as follows:

$$\mathrm{EVI} = 2.5 \times \frac{\rho_{\mathrm{nir}} - \rho_{\mathrm{red}}}{\rho_{\mathrm{nir}} + 6.0 \times \rho_{\mathrm{red}} - 7.5 \times \rho_{\mathrm{blue}} + 1}$$

where ρ_{nir}, ρ_{red}, and ρ_{blue} stand for the surface reflectances of the near-infrared, red band, and blue band.

Eucalyptus plantations exhibit a distinct pattern of EVI values over time, with a sharp decrease following clearcut events. To identify these clearcut events, we employed the sum of squared error (SSE) to partition a time series of EVI into harvest and regrowth segments over six-year spans [9]. Given the expected pronounced contrast in EVI values between these segments, the time exhibiting the lowest EVI value within each six-year window was tentatively identified as a potential clearcut event. Adjacent values were iteratively grouped into the harvest segment if their inclusion increased the overall SSE [see Fig. 4(a)]. The SSE was defined as follows:

$$\mathrm{SSE} = \sum_{i=1}^{N_h} \left(h_i - \bar{h}\right)^2 + \sum_{i=1}^{N_g} \left(g_i - \bar{g}\right)^2$$

where

h_i values in harvest segment;

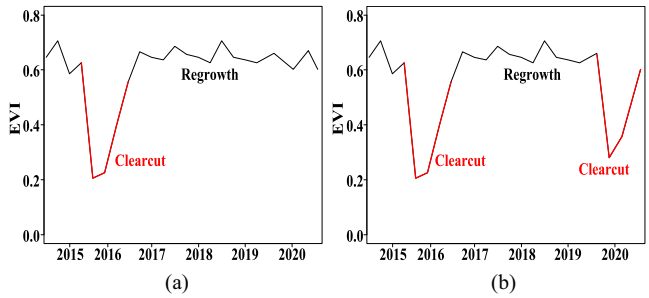

Fig. 4. Conceptual graph of time-series segmentation. The EVI time series in each pixel is divided into harvest (red) and regrowing (black) phases. While both Deng et al.'s [9] method and our modified clearcut-detection algorithm could successfully detect single clearcuts within a six-year observation window (Case a), our method demonstrates the unique capability to identify multiple clearcut events in Case b within the same time span (modified from [9] and [10]).

g_i values in the regrowth segment;
N_h count of observations in harvest segment;
N_g count of observations in regrowth segment;
$\bar{h}$ mean value of harvest segment;
$\bar{g}$ mean value of regrowth segment.

A one-tailed *t*-test was conducted to assess significant differences in EVI values between segmented regrowth and harvest parts. Clearcutting was inferred for pixels exhibiting a mean EVI value in the harvest segment significantly lower than the regrowth phase by a threshold of 0.12, as defined in [9]. Pixels not meeting this criterion were excluded from the clearcut classification.

The original Deng et al.'s [9] algorithm aimed to identify annual clearcut events within the six-year time span (2013–2018), regardless of whether the harvesting event occurred at the beginning, middle, or end of the time series. This approach might underestimate harvest events occurring twice in the six-year span, as SSE may not effectively separate one harvesting event from another mistakenly assumed to be a part of the regrowth phase [see Fig. 4(b)]. To mitigate this issue, we implemented a sliding time window approach to ensure that the year for identifying the harvest falls in the middle of the six-year time span, thereby reducing omission errors caused by the confounding effects of multiple harvesting events over the six-year time span. For instance, by analyzing EVI data from 1997 to 2002, clearcut events occurring exclusively in 1999 were isolated for subsequent analysis. This process was repeated for successive six-year intervals, generating annual clearcut distribution maps from 1999 to 2019.

D. Eucalyptus Classification

While time-series analysis effectively filters out nonclearcut events during the eucalyptus logging cycle, the pixels associated with at least a clearcut event during the six-year time span may not exclusively belong to eucalyptus plantations. These pixels could pertain to some other planted forests, such as pine and fir, that happened to undergo a clearcut in the preceding six years.

TABLE I
INFORMATION ABOUT TESTING SAMPLES

Year	Eucalyptus	Others	Total
2007	247	606	853
2010	491	595	1086
2015	862	761	1623
2019	2043	6535	8578

Therefore, further reclassification is essential to distinguish eucalyptus from other planted forests.

To circumvent misclassification issues driven by the bare ground and young saplings immediately (i.e., one- or two-year postharvest) following clearcuts, Landsat images acquired in the last year of each six-year sliding window (i.e., images taken three years after logging) were utilized to differentiate between eucalyptus and other planted forests. We evaluated four common classifiers—random forest, classification and regression tree, support vector machine, and minimum distance method—and determined random forest to be the superior choice for eucalyptus identification based on a pilot accuracy assessment. The model was trained on a dataset of 8578 samples, partially derived from the high-resolution Google Earth imagery and field sampling conducted in 2020 (see Table I).

Following the clearcut detection and eucalyptus classification, we aggregated the clearcut areas classified as eucalyptus within each six-year window into a single map, representing the eucalyptus distribution for that specific year (see Fig. 2). In other words, the eucalyptus clearcut maps from 1999 to 2004 were merged to create the eucalyptus distribution map in the year 2004, and this process was repeated for each subsequent six-year interval to generate annual potential eucalyptus distribution maps from 2004 to 2019.

E. Eucalyptus Plantation Mapping

To mitigate the misestimation issues of pixel-level classification for target feature identification based solely on standard time-series characteristics, we used the simple noniterative clustering (SNIC) image segmentation algorithm to consider the crucial role of spatial context in feature classification [33], [43]. This technique divides the landscape into segments (superpixels) with similar spectral characteristics, effectively capturing the spatial relationships between pixels [44]. The segmentation scale is a critical parameter influencing SNIC algorithm performance. Following Deng et al. [9], given our shared study area and Landsat imagery, we employed a two-tiered approach. Initial segmentation used a 10×10 pixels scale, followed by a 5×5-pixel subdivision for segments exceeding the median variance. This hierarchical strategy effectively delineated both small and large plantations.

After image segmentation, two threshold values should be estimated. We removed any segments whose size was less than 4 pixels (0.36 ha) to mitigate the salt–pepper effects (lower threshold). We deemed that such small patches were unlikely to be the plantation forest because, otherwise, the plantation cost would outweigh the timber value at such small scales. The upper threshold, representing the percentage of pixels within a segment identified as eucalyptus, was crucial for addressing potential omissions in large clearcuts. To determine this threshold, we leveraged provincial statistics on eucalyptus plantations [32], [34] and collected a 12-year record of plantation area from the forestry bureau's annual statistical reports. We iteratively adjusted upper thresholds ranging from 0% to 100% in increments of 1%, aiming to identify the value that led to eucalyptus area estimates closest to those reported plantation area statistics. Importantly, the optimal upper threshold varied across years. This variability reflects the evolving spatial patterns of eucalyptus plantation. Initially, plantations were scattered and discrete, leading to a higher optimal upper threshold for identifying dispersed eucalyptus pixels. As plantations expanded, forming contiguous distributions, a lower optimal upper threshold was more appropriate. This association allowed us to develop an empirical relationship between the optimal upper threshold and the landscape metrics describing the spatial patterns of eucalyptus plantation, which enabled us to estimate the appropriate upper threshold for years (i.e., years 2009, 2012, 2014, and 2018) lacking reported provincial-level eucalyptus plantation area statistics. We also calculated leverage values for each year's observation to quantify their influence on the model fit between the optimal upper threshold and the landscape metric. The landscape metrics were calculated in *Fragstats 4.2* [45].

F. Validating Eucalyptus Mapping

To evaluate the accuracy of our eucalyptus mapping, we employed two validation methods: Google Earth high-resolution imagery and field surveys (see Table I). Google Earth imagery offers reliable ground truthing for eucalyptus identification. However, it did not cover the entire study period (2004–2019). The visual interpretation was conducted for the years 2007, 2010, 2015, and 2019, during which the Google Earth imagery was available. We also conducted field surveys in year 2020 and 2021, collecting 3365 samplings across three land cover classes: eucalyptus plantations, croplands, and other vegetation types (e.g., orchard, pine, and fir). Since forests and croplands are relatively stable, these samples served as complimentary ground-truth data for validating eucalyptus map in the year 2019. For our research purpose, we classified land use into two categories: eucalyptus and noneucalyptus. We calculated the producer, user, and overall accuracy of the classification for each year of 2007, 2010, 2015, and 2019.

G. Eucalyptus Plantations Expansion Dynamics

To explore spatial expansion patterns, the percentage of eucalyptus planting area within each county was calculated for the years 2005, 2010, 2015, and 2019, highlighting the areas of high and low density. The influence of geological and topographic factors on these expansion patterns was also investigated to assess spatial heterogeneity. While eucalyptus prefers humid environments, the prevalent karst topography in Guangxi, characterized by inherent aridity [46], [47], may constrain its

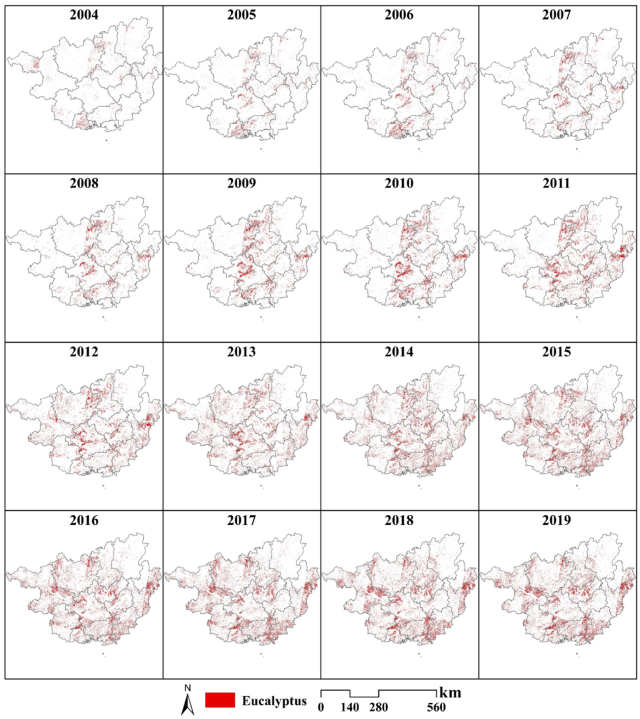

Fig. 5. Identified eucalyptus distribution maps from 2004 to 2019 across Guangxi, China.

TABLE II
CLASSIFICATION ACCURACY OF EUCALYPTUS PLANTATION MAPS

Year	UA (%)	PA (%)	OA (%)	Kappa
2007	82.74	65.99	86.17	0.64
2010	89.59	75.36	84.90	0.69
2015	94.35	87.12	80.72	0.81
2019	94.73	89.82	96.38	0.90

Note: UA: user's accuracy; PA: producer's accuracy; and OA: overall accuracy.

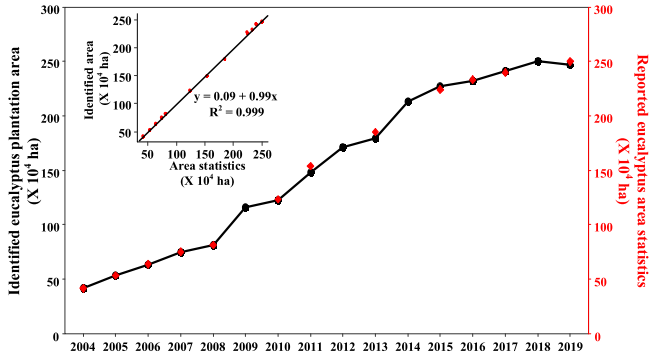

Fig. 6. Time series of identified eucalyptus plantation area and reported area statistics from 2004 to 2019.

expansion. Additionally, topographic features impact eucalyptus cultivation practices, growth rates, and harvesting efficiency, thereby affecting spatial patterns. We analyzed eucalyptus expansion within karst and nonkarst areas, as well as on gentle ($\leq$15°) and steep (>15°) slopes. Karst region delineation was sourced from the Institute of Karst Geology, Chinese Academy of Geological Sciences.[1] Slope map was derived from the shuttle radar topography mission digital elevation data with a 30-m spatial resolution [48].

IV. RESULTS

A. Eucalyptus Mapping Accuracy

This study developed annual eucalyptus plantation maps for Guangxi covering the period 2004–2019 (see Fig. 5). The eucalyptus mapping performance was assessed from both spatial and temporal perspectives. Testing samples from 2007, 2010, 2015, and 2019 were used to validate the identifying accuracy of eucalyptus plantations in the corresponding maps (see Table II). The validation results showed that user's accuracy exceeded 80% in all years. Notably, the user's accuracy surpassed the producer's accuracy across the four years, showing a minimal commission error.

We also compared the identified eucalyptus plantation area with corresponding area statistics reported by the forestry bureau (see Fig. 6). The comparison revealed a strong positive correlation ($R^2 = 0.999$, t-value < 0.01), indicating that both datasets captured the overall upward trend in eucalyptus plantation. Our results demonstrated the feasibility of time-series analysis-assisted eucalyptus plantation identification across a large scale.

B. Annual Eucalyptus Plantation Expansion From 2004 to 2019

Annual eucalyptus plantation distribution maps (see Fig. 5), alongside the chart in Fig. 6, clearly revealed the expansion dynamics of eucalyptus plantations across the region over the past 16 years. Between 2004 and 2015, eucalyptus plantations exhibited a rapid year-on-year expansion. This period witnessed a drastic surge in eucalyptus cover, as Fig. 6 clearly showcases. Interestingly, 2015 appeared to mark a potential turning point, with the expansion rate noticeably slowing down thereafter, suggesting a possible shift in dynamics.

Beyond the overall expansion rates, the spatial distribution revealed further insights. While central and southern Guangxi exhibited stable, contiguous plantations, a significant portion of the study area demonstrated dynamic changes with infrequent eucalyptus presence, occurring less than five times over the study period (see Fig. 7). These areas might represent newly established plantations or regions undergoing afforestation/reforestation initiatives. Fig. 8 also indicates a general northward expansion of eucalyptus plantations, ultimately encompassing the entire study area. While eucalyptus plantations in Northeastern Guangxi expanded at a slower pace, Central and Southern Guangxi experienced significantly faster growth, as illustrated in Figs. 7

1.[Online]. Available: http://en.cags.ac.cn/

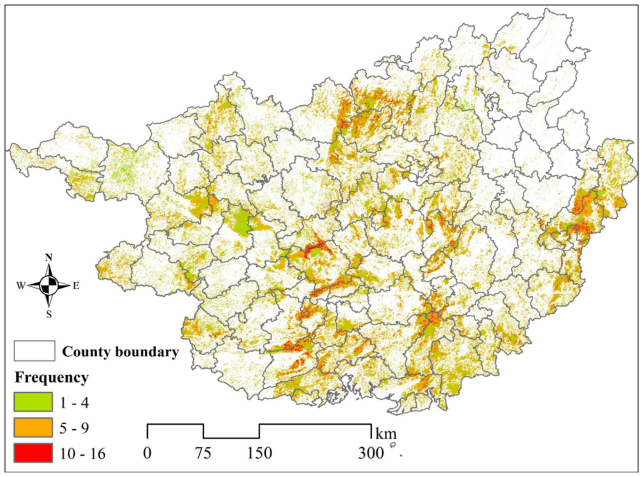

Fig. 7. Frequency of pixels classified as eucalyptus from 2004 to 2019.

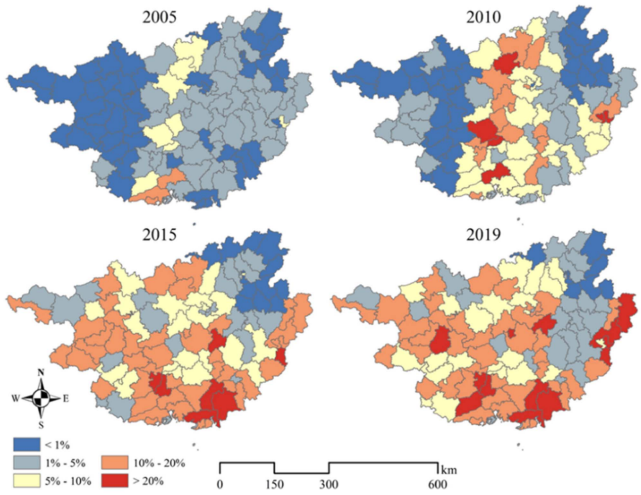

Fig. 8. County-level eucalyptus planting percentage for the years 2005, 2010, 2015, and 2019.

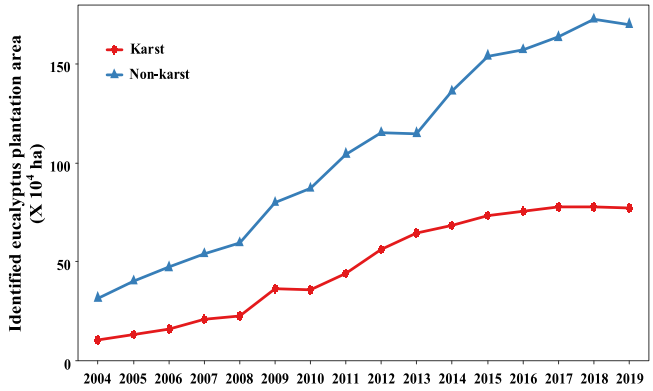

Fig. 9. Distribution of identified eucalyptus areas across karst and nonkarst regions from 2004 to 2019.

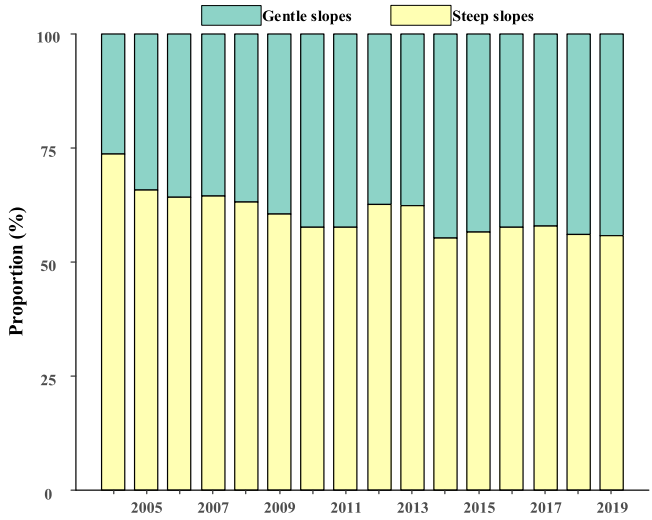

Fig. 10. Relative proportion of identified eucalyptus areas across gentle and steep slopes from 2004 to 2019.

and 8. This heterogeneity in expansion patterns underscored the influence of various ecological and socioeconomic factors operating across the region. Furthermore, Fig. 9 demonstrates that eucalyptus plantations primarily expanded within nonkarst regions, likely due to their generally more favorable ecological conditions. Fig. 10 reveals an interesting trend in the expansion of eucalyptus plantations from regions with steep terrain to those with more gentle slopes.

C. Estimating Upper Threshold in Image Segmentation

Our analysis revealed that the optimal upper threshold to determine the segment as a whole to be a eucalyptus plantation forest based on the percentage of pixels within a segment identified as eucalyptus exhibited a strong negative relationship with landscape metrics, particularly the shape index ($r = -0.74$, p-value < 0.01). This finding suggested that fragmented eucalyptus patches required a higher upper threshold for their identification compared with contiguous plantations. To leverage this relationship, we established a linear equation relating the upper threshold coefficient to the shape index (see Fig. 11). This model allowed us to estimate optimal upper thresholds for years without available statistical data of the province-level eucalyptus coverage, enabling continuous eucalyptus mapping throughout the study period. The effectiveness of this approach was validated through both classification accuracy and annual area dynamics analyses (see Table II and Fig. 6). Using the estimated upper thresholds resulted in highly accurate classifications and closely matched the observed annual changes in the eucalyptus area compared to years with statistical data. This confirmed the robustness of our model in predicting optimal upper thresholds for years lacking plantation area statistics.

V. Discussion

A. Advantage and Deficiency of This Method in Eucalyptus Plantation Identification

While previous studies have explored eucalyptus plantation identification in specific regions or years [28], [49], existing

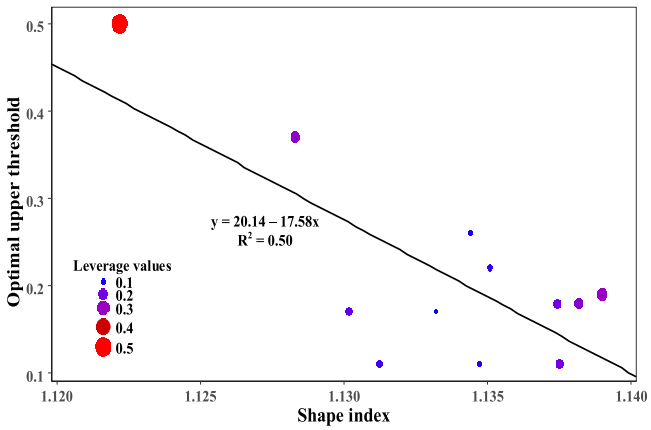

Fig. 11. Relationship between upper threshold and shape index. Circle size and color correspond to the leverage values of each data point, with larger and darker circles indicating greater influence on the regression model.

methods lack the efficiency and scalability required for large-scale, long-term monitoring. This gap is particularly critical for accurately capturing the rapid expansion of eucalyptus plantations and assessing their ecological service value as short-rotation timber forests. The primary challenge lies in the spectral similarity between eucalyptus and other timber species, such as spruce and pine. Classifying directly from images often leads to low classification accuracy. Fortunately, recent studies suggest that combining time-series analysis with spectrum or texture-based interpretation significantly improves classification performance [22], [50]. This highlights the need for new approaches that can further exploit the power of time-series data to effectively monitor large-scale eucalyptus plantation dynamics. Our study aimed to address this gap by establishing a robust methodology that combines time-series analysis with spectral classification relying solely on a single remote sensing data source to map and analyze annual eucalyptus plantations across an extended period. By analyzing time series of medium-resolution satellite imagery, such as Landsat data, we can exploit the unique spectral characteristics of these fast-growing plantations to identify their expansion patterns over time. The resulting data will provide valuable insights into the ecological implications of eucalyptus plantations and inform the development of effective forest management strategies.

Our study leveraged both the multispectral characteristics of eucalyptus plantations and their temporal dynamics for identification. We employed a time-series analysis to detect clearcuts every six years, creating potential eucalyptus distribution maps. However, this approach could initially include harvests from long-rotation timber forests, such as spruce and pine. Fortunately, the disparity in harvest cycles provides a valuable tool for discrimination. Spruce and pine typically have harvest cycles exceeding 20 years, meaning they would only be detected as clearcuts once during our entire study period (2004–2019) and even less frequently within each six-year interval. This characteristic helped us filter out false positives and improve the accuracy of subsequent eucalyptus classification.

While the typical rotation cycle for fast-growing eucalyptus falls between 4 and 6 years, it possibly stretches from 3 to 8 years. This variability presents a challenge for our approach of overlaying clearcut maps every six years to create potential eucalyptus distribution maps. Longer rotation plantations may be inadvertently omitted (see Fig. 7). To address this limitation, future research can explore smoothing algorithms that identify pixels as eucalyptus if they are classified as such in neighboring years. However, it is important to acknowledge another potential source of uncertainty: unharvested eucalyptus plantations. The increasing focus on the ecological impacts of short-rotation eucalyptus may incentivize some landowners to adopt longer cycles or forego harvesting altogether. Therefore, accounting for unharvested plantations will be crucial for the accurate eucalyptus identification in future studies.

The fragmented ownership and piecemeal logging of eucalyptus plantations by small landholders create a highly heterogeneous landscape of clearcuts. This poses a challenge for classification accuracy, as coarser scale remote sensing data, such as Landsat's 30-m resolution, might miss smaller plantation patches. The subsequent image segmentation refinement can potentially offset this limitation. However, cloud contamination can limit the acquisition of sufficient cloud-free observations for continuous EVI time series across each pixel [51]. This issue can hinder the effectiveness of clearcut-detection algorithms (see Fig. 3), ultimately restricting the planted forest mapping. The increasing availability of diverse remote sensing data sources provides a potential solution to address this deficiency through multisource data fusion. Nevertheless, for historical eucalyptus mapping, this approach remains constrained by the limited temporal coverage of newly launched satellite datasets.

Expanding upon the standard EVI-based eucalyptus identification, image segmentation further refined the results and alleviated misclassification errors induced by noisy or mixed-pixel time series. However, this technique presents a tradeoff. It may inadvertently exclude small and fragmented eucalyptus patches, especially during the initial expansion stage characterized by a scattered distribution pattern. This effect is expected to diminish as plantations mature and become more contiguous. Furthermore, image segmentation can exacerbate commission errors (false positives) in the clearcut-detection model. Utilizing a consistent upper threshold for segmentation can amplify this issue in eucalyptus distribution mapping. Our study underscores the sensitivity of image segmentation thresholds to changes in landscape pattern variations, highlighting their nonuniformity across the study period. Although employing dynamic coefficients improved the final accuracy of identified plantation areas, these coefficients were determined empirically in this work, necessitating further refinement.

Threshold determination for vegetation identification within time-series data remains challenging [52]. While spectral similarity-based methods [53], [54] and statistical data-driven approaches [32], [42], [55] have been explored, both methods present limitations. Spectral similarity methods often require extensive ground-truth data and are susceptible to data quality issues, hindering large-scale application. Despite their efficiency, statistical data-driven approaches risk introducing biases

that can lead to inaccurate or incomplete vegetation identification. Our hybrid approach, combining image segmentation and statistical-derived thresholds, achieves satisfactory accuracy without extensive ground-truth data. While acknowledging potential biases, this method offers a practical, cost-effective solution for large-scale monitoring. However, the reliance on statistical data warrants further exploration of alternative thresholding methods incorporating spectral and phenological information to enhance accuracy and robustness.

B. Spatial Distribution of Eucalyptus Plantations

Over the past 16 years, eucalyptus plantations in Guangxi have experienced a substantial expansion, with the bulk of this expansion concentrated in the central and southern regions (see Figs. 5 and 8). This pattern can be attributed to a complex interplay of environmental factors, economic considerations, and historical planting practices. Optimal climatic conditions for eucalyptus growth likely played a key role in driving expansion in the central and southern parts. Notably, the extensive karst terrain with exposed bedrock in the northern region may render it less suitable for eucalyptus cultivation, potentially explaining the observed lower plantation density there (see Fig. 9).

Initially, eucalyptus plantations were established primarily in upland areas, reflecting their introduction and initial cultivation strategies (see Fig. 10). Subsequent expansion targeted flatter terrains. However, economic considerations and labor intensity relative to other crops ultimately regulated the pace of expansion across different topographic zones. Thus, the observed distribution of eucalyptus plantations often deviates from their ideal elevation and slope ranges. While expansion into higher altitude and steeper slopes regions has occurred, a gradual concentration of plantations on low-elevation, gentle slopes is also evident. This trend raises concerns about potential conflicts with agriculture land use in these areas.

C. Implication for Timber Forest Management

While previous studies had made great efforts to track the land cover conversion of tropical forests, the spatiotemporal expansion of timber plantations, particularly at large scales, has received less attention. Driven by increasing wood demand, timber plantations are expanding, often at the expense of natural forests. This trend is evident in Guangxi, where our analyses show that eucalyptus plantations have increased from 0.42×10^6 ha in 2004 to approximately 2.47×10^6 ha in 2019. This rapid expansion raises concerns about potential ecological and environmental consequences. Despite control efforts by the Guangxi Forestry Ministry regarding short-rotation eucalyptus cultivation, high economic returns continue to drive the expansion. This practice, often involving monoculture and successive planting, is linked to soil degradation and biodiversity loss [5], [56]. For sustaining the development of planted forests and mitigating conflicts with other land uses, we advocate to enhance forest management of the existing plantations by intercropping with native tree species [57] and stretching cutting cycle [58], [59], [60]. In the meantime, plantation expansion should be strictly limited to avoid encroachment on agricultural land or natural forests. Furthermore, developing more segregated eucalyptus plantation patches would be helpful for wildlife conservation and wood production. By implementing these strategies, Guangxi can achieve responsible expansion and management of eucalyptus plantations, and ensure a balance between economic benefits and ecological integrity for a sustainable future.

VI. Conclusion

This study leverages the distinct temporal phenology patterns of short-rotation plantations to map the spatiotemporal dynamics of eucalyptus across Guangxi province, China. Initial detection relied on Landsat EVI variations before and after timber harvests, effectively identifying clearcuts within eucalyptus plantations. This approach minimizes confusion with long-rotation timber forests (i.e., pine and fir) due to their infrequent harvests ($>$ 20 years), significantly reducing classification errors. Clearcut eucalyptus pixels were further confirmed through spectral classification based on the detailed spectral information. Subsequently, image segmentation refined the identified eucalyptus distribution to mitigate misclassifications arising from landscape heterogeneity in planting patterns and logging schedules. The resulting maps captured the long-term spatiotemporal eucalyptus expansion dynamics across Guangxi with high accuracy. However, limitations associated with the eucalyptus distribution maps remain. Major limitations include the limited availability of high-quality Landsat images caused by frequent cloudy and rainy weather, and the mixed-pixel issue, especially in areas where eucalyptus plantations are managed by smallholders. These limitations might be addressed through multisensor data fusion. Overall, our time-series analysis successfully captured the spatial and temporal dynamics of eucalyptus plantations in Guangxi, providing a robust and reliable depiction of their extent and growth trends. This information can be valuable for understanding the ecological and socioeconomic implications of eucalyptus plantations in the region. With further refinements and data integration, the method developed in this study holds promise for monitoring short-rotation timber forests across large scales, thereby supporting sustainable forest management practices.

Acknowledgment

The authors would like to thank Google Earth Engine for providing the geospatial datasets and the date processing platform, X. Deng for sharing clearcut detection algorithms, and the two anonymous reviewers and the academic editor for their constructive comments and suggestions, which have greatly improved the quality of this article.

References

[1] J.-P. Laclau, J. L. de Moraes Gonçalves, and J. L. Stape, "Perspectives for the management of eucalypt plantations under biotic and abiotic stresses," *Forest Ecol. Manage.*, vol. 301, pp. 1–5, 2013.

[2] A. Paquette and C. Messier, "The role of plantations in managing the world's forests in the Anthropocene," *Front. Ecol. Environ.*, vol. 8, pp. 27–34, 2010.

[3] R. L. Chazdon et al., "Carbon sequestration potential of second-growth forest regeneration in the Latin American tropics," *Sci Adv.*, vol. 2, 2016, Art. no. e1501639.

[4] X. Tong et al., "Forest management in southern China generates short term extensive carbon sequestration," *Nature Commun.*, vol. 11, 2020, Art. no. 129.

[5] Z. Yu et al., "Natural forests exhibit higher carbon sequestration and lower water consumption than planted forests in China," *Glob. Change Biol.*, vol. 25, pp. 68–77, 2019.

[6] D. Lemessa et al., "Do eucalyptus plantation forests support biodiversity conservation?," *Forest Ecol. Manage.*, vol. 523, 2022, Art. no. 120492.

[7] C. Zhang et al., "Effects of eucalyptus litter and roots on the establishment of native tree species in eucalyptus plantations in South China," *Forest Ecol. Manage.*, vol. 375, pp. 76–83, 2016.

[8] Z. Yu, W. You, E. Agathokleous, G. Zhou, and S. Liu, "Forest management required for consistent carbon sink in China's forest plantations," *Forest Ecosyst.*, vol. 8, 2021, Art. no. 54.

[9] X. Deng, S. Guo, L. Sun, and J. Chen, "Identification of short-rotation eucalyptus plantation at large scale using multi-satellite imageries and cloud computing platform," *Remote Sens.*, vol. 12, 2020, Art. no. 2153.

[10] H. Qiao, M. Wu, M. Shakir, L. Wang, J. Kang, and Z. Niu, "Classification of small-scale eucalyptus plantations based on NDVI time series obtained from multiple high-resolution datasets," *Remote Sens.*, vol. 8, no. 2, 2016, Art. no. 117.

[11] H. Zhao et al., "Mapping the distribution of invasive tree species using deep one-class classification in the tropical montane landscape of Kenya," *ISPRS J. Photogramm. Remote Sens.*, vol. 187, pp. 328–344, 2022.

[12] Y. Cheng et al., "Mapping oil palm plantation expansion in Malaysia over the past decade (2007–2016) using ALOS-1/2 PALSAR-1/2 data," *Int. J. Remote Sens.*, vol. 40, pp. 7389–7408, 2019.

[13] G. le Maire et al., "MODIS NDVI time-series allow the monitoring of eucalyptus plantation biomass," *Remote Sens. Environ.*, vol. 115, pp. 2613–2625, 2011.

[14] L. Wu et al., "Multi-type forest change detection using BFAST and monthly Landsat time series for monitoring spatiotemporal dynamics of forests in subtropical wetland," *Remote Sens.*, vol. 12, no. 2, 2020, Art. no. 341.

[15] R. Dong et al., "Oil palm plantation mapping from high-resolution remote sensing images using deep learning," *Int. J. Remote Sens.*, vol. 41, pp. 2022–2046, 2020.

[16] J. Hemmerling, D. Pflugmacher, and P. Hostert, "Mapping temperate forest tree species using dense Sentinel-2 time series," *Remote Sens. Environ.*, vol. 267, 2021, Art. no. 112743.

[17] A. Hościło and A. Lewandowska, "Mapping forest type and tree species on a regional scale using multi-temporal Sentinel-2 data," *Remote Sens.*, vol. 11, no. 8, 2019, Art. no. 929.

[18] M. Dalponte, L. Bruzzone, and D. Gianelle, "Tree species classification in the Southern Alps based on the fusion of very high geometrical resolution multispectral/hyperspectral images and LiDAR data," *Remote Sens. Environ.*, vol. 123, pp. 258–270, 2012.

[19] J. Dong et al., "Mapping deciduous rubber plantations through integration of PALSAR and multi-temporal Landsat imagery," *Remote Sens. Environ.*, vol. 134, pp. 392–402, 2013.

[20] L. Wan, Y. Lin, H. Zhang, F. Wang, M. Liu, and H. Lin, "GF-5 hyperspectral data for species mapping of mangrove in Mai Po, Hong Kong," *Remote Sens.*, vol. 12, no. 4, 2020, Art. no. 656.

[21] Y. Cheng et al., "Towards global oil palm plantation mapping using remote-sensing data," *Int. J. Remote Sens.*, vol. 39, pp. 5891–5906, 2018.

[22] M. E. Fagan et al., "Mapping pine plantations in the southeastern U.S. using structural, spectral, and temporal remote sensing data," *Remote Sens. Environ.*, vol. 216, pp. 415–426, 2018.

[23] C. D. Kummerow et al., "Hyperspectral microwave sensors—Advantages and limitations," *IEEE J. Sel. Topics Appl. Earth Observ. Remote Sens.*, vol. 15, pp. 764–775, Jan. 2022.

[24] V. J. Pasquarella, C. E. Holden, and C. E. Woodcock, "Improved mapping of forest type using spectral-temporal Landsat features," *Remote Sens. Environ.*, vol. 210, pp. 193–207, 2018.

[25] X. Zhu and D. Liu, "Accurate mapping of forest types using dense seasonal Landsat time-series," *ISPRS J. Photogramm. Remote Sens.*, vol. 96, pp. 1–11, 2014.

[26] G. le Maire, S. Dupuy, Y. Nouvellon, R. A. Loos, and R. Hakamada, "Mapping short-rotation plantations at regional scale using MODIS time series: Case of eucalypt plantations in Brazil," *Remote Sens. Environ.*, vol. 152, pp. 136–149, 2014.

[27] L. Fang, J. Yang, Wenqiu Zhang, W. Zhang, and Q. Yan, "Combining allometry and Landsat-derived disturbance history to estimate tree biomass in subtropical planted forests," *Remote Sens. Environ.*, vol. 235, 2019, Art. no. 111423.

[28] B. Yang, Y. Zhang, X. Mao, Y. Lv, F. Shi, and M. Li, "Mapping spatiotemporal changes in forest type and aboveground biomass from Landsat long-term time-series analysis—A case study from Yaoluoping National Nature Reserve, Anhui Province of Eastern China," *Remote Sens.*, vol. 14, no. 12, 2022, Art. no. 2786.

[29] G. W. Meigs, R. E. Kennedy, and W. B. Cohen, "A Landsat time series approach to characterize bark beetle and defoliator impacts on tree mortality and surface fuels in conifer forests," *Remote Sens. Environ.*, vol. 115, pp. 3707–3718, 2011.

[30] D. Pflugmacher, W. B. Cohen, and R. E. Kennedy, "Using Landsat-derived disturbance history (1972-2010) to predict current forest structure," *Remote Sens. Environ.*, vol. 122, pp. 146–165, 2012.

[31] K. C. Rodman, R. A. Andrus, T. T. Veblen, and S. J. Hart, "Disturbance detection in Landsat time series is influenced by tree mortality agent and severity, not by prior disturbance," *Remote Sens. Environ.*, vol. 254, 2021, Art. no. 112244.

[32] R. Shen, J. Dong, W. Yuan, W. Han, T. Ye, and W. Zhao, "A 30 m resolution distribution map of maize for China based on Landsat and sentinel images," *J. Remote Sens.*, vol. 2022, 2022, Art. no. 9846712.

[33] R. Achanta and S. Susstrunk, "Superpixels and polygons using simple non-iterative clustering," in *Proc. IEEE Conf. Comput. Vis. Pattern Recognit.*, Honolulu, HI, USA, 2017, pp. 4895–4904.

[34] Q. Peng et al., "A twenty-year dataset of high-resolution maize distribution in China," *Sci. Data*, vol. 10, no. 1, 2023, Art. no. 658.

[35] Z. Lu, "Eucalyptus: Past, present, and future," *Forestry Guangxi*, no. 12, pp. 18–25, 2021 (In Chinese).

[36] D. Tian et al., "A long-term evaluation of biomass production in first and second rotations of Chinese fir plantations at the same site," *Forestry*, vol. 84, pp. 411–418, 2011.

[37] Z. Ying et al., "Plantation development: Economic analysis of forest management in Fujian Province, China," *Forest Policy Econ.*, vol. 12, no. 3, pp. 223–230, 2010.

[38] N. T. Son, C. F. Chen, C. R. Chen, V. Q. Minh, and N. H. Trung, "A comparative analysis of multitemporal MODIS EVI and NDVI data for large-scale rice yield estimation," *Agricultural Forest Meteorol.*, vol. 197, pp. 52–64, 2014.

[39] Y. Setiawan, K. Yoshino, and L. B. Prasetyo, "Characterizing the dynamics change of vegetation cover on tropical forestlands using 250m multitemporal MODIS EVI," *Int. J. Appl. Earth Observ. Geoinf.*, vol. 26, pp. 132–144, 2014.

[40] J. Hua, G. Chen, L. Yu, Q. Ye, H. Jiao, and X. Luo, "Improved mapping of long-term forest disturbance and recovery dynamics in the subtropical China using all available Landsat time-series imagery on Google Earth engine platform," *IEEE J. Sel. Topics Appl. Earth Observ. Remote Sens.*, vol. 14, pp. 2754–2768, Feb. 2021.

[41] T. H. Nguyen, S. D. Jones, M. Soto-Berelov, A. Haywood, and S. Hislop, "A spatial and temporal analysis of forest dynamics using Landsat time-series," *Remote Sens. Environ.*, vol. 217, pp. 461–475, 2018.

[42] K. Xiang, W. Yuan, L. Wang, and Y. Deng, "An LSWI-based method for mapping irrigated areas in China using moderate-resolution satellite data," *Remote Sens.*, vol. 12, 2020, Art. no. 4181.

[43] M. Hussain, D. Chen, A. Cheng, H. Wei, and D. Stanley, "Change detection from remotely sensed images: From pixel-based to object-based approaches," *ISPRS J. Photogramm. Remote Sens.*, vol. 80, pp. 91–106, 2013.

[44] C. Li, B. Guo, G. Wang, Y. Zheng, Y. Liu, and W. He, "NICE: Superpixel segmentation using non-iterative clustering with efficiency," *Appl. Sci.*, vol. 10, no. 12, 2020, Art. no. 4415.

[45] K. McGarigal, S. A. Cushman, M. C. Neel, and E. Ene, *FRAGSTATS: Spatial Pattern Analysis Program for Categorical Maps*. Amherst, MA, USA: Univ. of Massachusetts, 2002.

[46] D. Ford and P. D. Williams, *Karst Hydrogeology and Geomorphology*. Hoboken, NJ, USA: Wiley, 2007.

[47] K. Wang et al., "Karst landscapes of China: Patterns, ecosystem processes and services," *Landscape Ecol.*, vol. 34, pp. 2743–2763, 2019.

[48] T. G. Farr et al., "The shuttle radar topography mission," *Rev. Geophys.*, vol. 45, 2007, Art. no. RG2004.

[49] C. Li et al., "A circa 2010 thirty meter resolution forest map for China," *Remote Sens.*, vol. 6, no. 6, pp. 5325–5343, 2014.

[50] L. Sun, J. Chen, S. Guo, X. Deng, and Y. Han, "Integration of time series Sentinel-1 and Sentinel-2 imagery for crop type mapping over oasis agricultural areas," *Remote Sens.*, vol. 12, no. 1, 2020, Art. no. 158.
[51] K. Turlej, M. Ozdogan, and V. C. Radeloff, "Mapping forest types over large areas with Landsat imagery partially affected by clouds and SLC gaps," *Int. J. Appl. Earth Observ. Geoinf.*, vol. 107, 2022, Art. no. 102689.
[52] S. Lhermitte, J. Verbesselt, W. W. Verstraeten, and P. Coppin, "A comparison of time series similarity measures for classification and change detection of ecosystem dynamics," *Remote Sens. Environ.*, vol. 115, pp. 3129–3152, 2011.
[53] I. W. Nuarsa, F. Nishio, C. Hongo, and I. G. Mahardika, "Using variance analysis of multitemporal MODIS images for rice field mapping in Bali Province, Indonesia," *Int. J. Remote Sens.*, vol. 33, pp. 5402–5417, 2012.
[54] Y. Meng, B. Hou, C. Ding, L. Huang, Y. Guo, and Z. Tang, "Spatiotemporal patterns of planted forests on the Loess plateau between 1986 and 2021 based on Landsat NDVI time-series analysis," *GIScience Remote Sens.*, vol. 60, 2023, Art. no. 2185980.
[55] J. Dong et al., "Early-season mapping of winter wheat in China based on Landsat and Sentinel images," *Earth Syst. Sci. Data*, vol. 12, pp. 3081–3095, 2020.
[56] S. C. Cunningham et al., "Reforestation with native mixed-species plantings in a temperate continental climate effectively sequesters and stabilizes carbon within decades," *Glob. Change Biol.*, vol. 21, pp. 1552–1566, 2015.
[57] S. Chu et al., "Effects of enriched planting of native tree species on surface water flow, sediment, and nutrient losses in a eucalyptus plantation forest in southern China," *Sci. Total Environ.*, vol. 675, pp. 224–234, 2019.
[58] S. Haberstroh and C. Werner, "The role of species interactions for forest resilience to drought," *Plant Biol.*, vol. 24, pp. 1098–1107, 2022.
[59] M. Pardos et al., "The greater resilience of mixed forests to drought mainly depends on their composition: Analysis along a climate gradient across Europe," *Forest Ecol. Manage.*, vol. 481, 2021, Art. no. 118687.
[60] Z. Yu, G. Zhou, S. Liu, P. Sun, and E. Agathokleous, "Impacts of forest management intensity on carbon accumulation of China's forest plantations," *Forest Ecol. Manage.*, vol. 472, 2020, Art. no. 118252.